


# Enhancing the Refractive Index of Polymers with a Plant-Based Pigment

## Journal Article

### Author(s):

Yasir, Mohammad; Sai, Tianqi; Sicher, Alba ; Scheffold, Frank; Steiner, Ullrich; Wilts, Bodo D.; Dufresne, Eric R.

### Publication date:

2021-11-04

### Permanent link:

<https://doi.org/10.3929/ethz-b-000507675>

### Rights / license:

[Creative Commons Attribution-NonCommercial-NoDerivatives 4.0 International](#)

### Originally published in:

Small 17(44), <https://doi.org/10.1002/smll.202103061>

# Enhancing the Refractive Index of Polymers with a Plant-Based Pigment

Mohammad Yasir, Tianqi Sai, Alba Sicher, Frank Scheffold, Ullrich Steiner, Bodo D. Wilts, and Eric R. Dufresne\*


Polymers are essential components of many nanostructured materials. However, the refractive indices of common polymers fall in a relatively narrow range between 1.4 and 1.6. Here, it is demonstrated that loading commercially-available polymers with large concentrations of a plant-based pigment can effectively enhance their refractive index. For polystyrene (PS) loaded with 67 w/w%  $\beta$ -carotene (BC), a peak value of 2.2 near the absorption edge at 531 nm is achieved, while maintaining values above 1.75 across longer wavelengths of the visible spectrum. Despite high pigment loadings, this blend maintains the thermoforming ability of PS, and BC remains molecularly dispersed. Similar results are demonstrated for the plant-derived polymer ethyl cellulose (EC). Since the refractive index enhancement is intimately connected to the introduction of strong absorption, it is best suited to applications where light travels short distances through the material, such as reflectors and nanophotonic systems. Enhanced reflectance from films is experimentally demonstrated, as large as sevenfold for EC at selected wavelengths. Theoretical calculations highlight that this simple strategy can significantly increase light scattering by nanoparticles and enhance the performance of Bragg reflectors.

## 1. Introduction

Polymers are widely employed in nanostructured materials because they can self-assemble into a wide variety of

M. Yasir, T. Sai, A. Sicher, E. R. Dufresne  
Department of Materials  
ETH Zürich  
8093 Zürich, Switzerland  
E-mail: eric.dufresne@mat.ethz.ch

F. Scheffold  
Department of Physics  
University of Fribourg  
1700 Fribourg, Switzerland  
U. Steiner, B. D. Wilts  
Adolphe Merkle Institute  
University of Fribourg  
1700 Fribourg, Switzerland

 The ORCID identification number(s) for the author(s) of this article can be found under <https://doi.org/10.1002/smll.202103061>.

© 2021 The Authors. Small published by Wiley-VCH GmbH. This is an open access article under the terms of the Creative Commons Attribution-NonCommercial-NoDerivs License, which permits use and distribution in any medium, provided the original work is properly cited, the use is non-commercial and no modifications or adaptations are made.

DOI: 10.1002/smll.202103061

well-controlled structures.<sup>[1]</sup> Even though many of these structures could be very attractive for optical applications, their performance is limited by the relatively low refractive index of common polymers, which is typically between 1.4 and 1.6. To that end, considerable effort has been invested in the development of high refractive index polymers and/or polymer composites.<sup>[2–13]</sup>

Methods to prepare high refractive index materials can be classified into three approaches. First, monomers are chemically modified to incorporate heavy atoms such as sulfur.<sup>[14–16]</sup> This can be synthetically tedious and costly. A polymer synthesized from vapor phase radical polymerization of elemental sulfur and 1,4-butanediol divinyl ether appears to have the highest refractive index reported for such a specialty polymer, with a value of about 2.1 at the wavelength of 400 nm, decaying to 1.9 at 700 nm.<sup>[15]</sup> Second, high refractive index particles are dispersed

throughout the polymer matrix. These are typically nanoparticles (NPs) of metal oxides such as zirconium oxide or titanium dioxide. This approach is challenging because the particles need to be small and well-dispersed to avoid light scattering, while their high surface energies tend to drive agglomeration.<sup>[7,13,17]</sup> For these composite materials, refractive indices as high as 2.5 have been reported for 60% of PbS in gelatin.<sup>[18]</sup> Polymers loaded by metallic nanoparticles can also display an elevated refractive index in the vicinity of plasmon resonances, and display enhanced reflectance.<sup>[19]</sup> Third, small absorbing molecules can be dispersed in the polymer matrix. To date, this approach has focused on pigments with absorption in the UV, like phenanthrene, providing modest increases of the refractive index,  $\Delta n$ , of about 0.07 across the visible range.<sup>[20–23]</sup>

Pigments and other absorbing systems can naturally feature high refractive indices. This is due the fact that both absorption and the refractive index are derived from the same linear response function, the dielectric constant. Basic constraints on causality require the refractive index (related to the real part of the response function) and the absorption coefficient (related to the imaginary part) to be connected through the Kramers–Kronig relationship.<sup>[24]</sup> This is famously exploited in silicon photonics, where the refractive index is about 3.5 beyond the band gap.<sup>[25–27]</sup> Recently, larger-scale organization of resonators has been shown to enhance these effects. For example, self-assembled films of

gold nanoparticles were shown to maintain refractive indices as high as 4.5, even far from resonance (in the mid-infrared).<sup>[28]</sup>

Living systems can achieve very high refractive indices using organic pigments. Melanin has a refractive index of about 1.8 and is deployed in nanostructures by many species to produce structural colors.<sup>[29–31]</sup> Artificial melanin has been used to create structurally colored biomimetic nanostructures.<sup>[32,33]</sup> Pterin pigments, which absorb strongly at short wavelengths, have recently been identified as an essential component of highly reflective structures in animals.<sup>[34,35]</sup> For example, the wing scales *Pierid* butterflies carry micron-sized ellipsoidal particles made primarily from pterin pigments. These particles have refractive indices as high as 2.9 at the edge of the absorption band, and remain above 2.0 at longer wavelengths.<sup>[34]</sup> In this region of the spectrum, the high refractive index of these nanostructures leads to very efficient reflection.

Here, we increase the refractive index of the common polymers polystyrene (PS) and ethyl cellulose (EC) by loading them the natural organic pigment  $\beta$ -carotene (BC). We achieve refractive indices greater than two near the absorption edge, while maintaining the processability of the host polymer. All of these raw materials are produced commercially and made from naturally abundant elements (carbon, hydrogen, and oxygen). Moreover, BC and EC are plant-based edible materials. Thus, our high-refractive-index materials are cost-effective, sustainable, and environmental friendly. Because of residual adsorption, these materials are best suited for applications where light travels no more than several wavelengths through the material. We demonstrate the applicability of this approach with a combination of experiments and theory. First, we measure increases of reflectance from flat interfaces as large as sevenfold greater than the base polymer. Second, we theoretically investigate the performance of nanoparticles and nanostructures based on these materials. Specifically, we find that pigment loading greatly enhances the reflectance of a multilayer structure and the scattering efficiency of nanoparticles.

## 2. Results and Discussion

In order to enhance the refractive index of polymeric materials using a pigment, it must satisfy two minimal criteria: i) it must have a strong optical response and ii) it can be dispersed in the desired polymeric matrix.

Since pigments are usually characterized by their absorption spectrum and not their refractive index, we applied the Kramers–Kronig relations (see e.g., refs. [24,36]) to estimate the impact of dye loading on the refractive index. The change in the refractive index due to absorption can be estimated as:

$$\Delta n(\lambda) = \frac{c}{2\pi^2} \int_0^{\infty} \frac{\mathcal{E}(\lambda')}{1 - (\lambda'/\lambda)^2} d\lambda' \quad (1)$$

where  $\mathcal{E}(\lambda)$  is the molar extinction coefficient of the pigment and  $c$  is its molar concentration.<sup>[36]</sup> The numerical approach to the evaluation of this integral is given in the Supporting Information.

Qualitatively, the refractive index increases with the molar extinction coefficient. Absorption over a narrow band of wavelengths

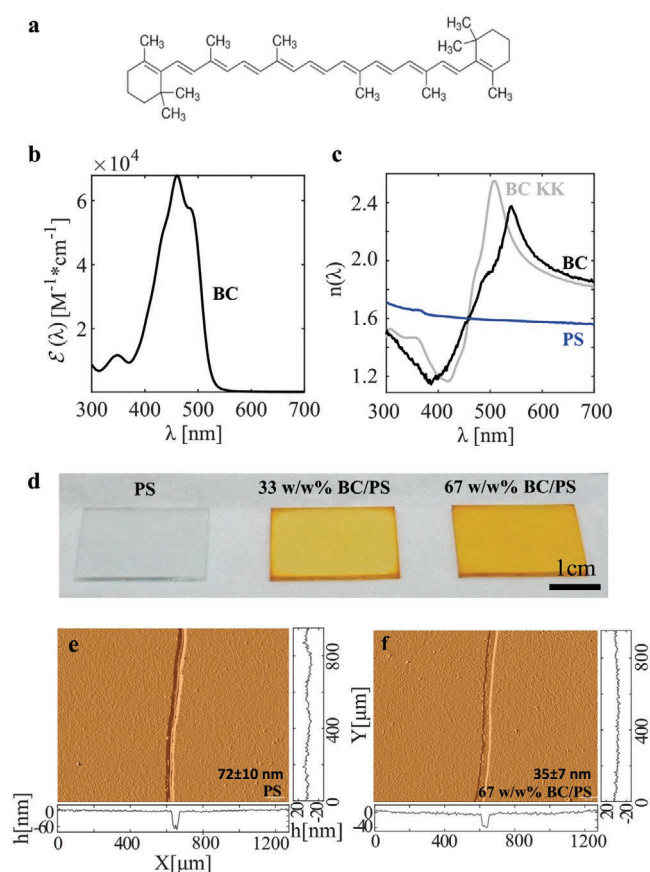


**Figure 1.** Design principle. a) Chemical structure of BC. b) Molar extinction coefficient of 0.1 mM BC in chloroform. c) Measured refractive indices of the spin-coated pure BC film (black) and the spin-coated PS film (blue). Estimated refractive indices of pure BC by using the Kramers–Kronig (KK) relationship (gray). d) Photos of spin-coated PS on glass slides with BC-loadings of 0, 33, 67 w/w% (size: 2.5 × 2.2 cm<sup>2</sup>). e, f) Profilometer images of PS and 67 w/w% BC/PS films and corresponding height profiles.

results in a peak of the refractive index at the long-wavelength edge of the absorption band.<sup>[36]</sup> The refractive index decays slowly at longer wavelengths. An ideal pigment to enhance the refractive index would feature an absorption spectrum with a large integral and a sharp drop to zero at long wavelengths.

We identified  $\beta$ -carotene, shown in **Figure 1a**, as a suitable candidate based on its absorption spectrum, shown in **Figure 1b**. Solutions of BC in chloroform absorb strongly between 400 and 550 nm, with a peak molar extinction coefficient of about 68 000 M<sup>-1</sup> cm<sup>-1</sup> at 460 nm. In addition to these suitable absorption properties, BC is a healthy and abundant natural product, soluble in a variety of common solvents.

The absorption spectrum of BC implies that it should have a large refractive index. To measure this, we spin-coated a 145 nm thick film of BC on a silicon wafer and measured its refractive index using an ellipsometer. The measured refractive index is shown as the black line in **Figure 1c**. A peak refractive index of 2.38 is observed at a wavelength of 541 nm. The refractive index stays above 2.0 up to a wavelength of 600 nm, well outside of its absorption band. At this wavelength, the residual absorption is 276 M<sup>-1</sup> cm<sup>-1</sup>, about 250× smaller than its peak value.

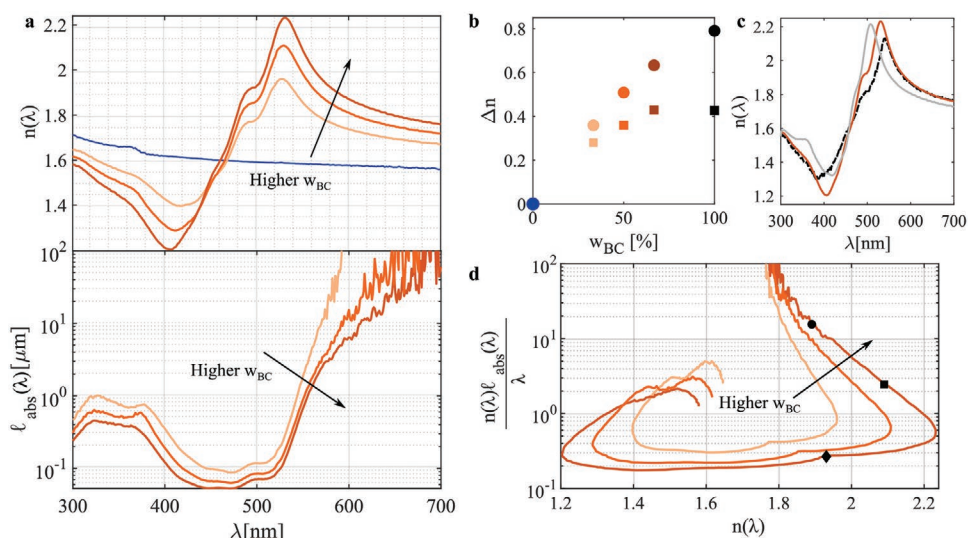


**Figure 2.** Trade-off between high refractive index and absorption. a) Measured refractive index dispersion and absorption lengths of BC-containing PS films with loading of 67, 50, and 33 w/w% and pure PS (blue). b) Peak refractive indices (circles) and refractive indices when  $n(\lambda)\ell_{\text{abs}} = 5\lambda$  (squares) for different weight percentage BC-containing PS films. c) Calculated and measured refractive indices of 67 w/w% BC/PS film. Measured in solid, orange line, calculated by mixing rule in black, dashed line and calculated by Kramers–Kronig in light gray, solid line. d) Normalized absorption length versus refractive indices for 67 w/w% BC/PS film, 50 w/w% BC/PS film, and 33 w/w% BC/PS film. Data points of 67 w/w% BC/PS for wavelengths of 500, 535, and 592 nm are marked in diamond, square, and circle, respectively.

For comparison, the refractive index predicted by the measured absorption spectrum using Equation (1) is shown as a gray line in Figure 1c. Note that the measured peak in the refractive index is weaker and at a longer wavelength than expected. We suspect that these differences arise from changes in the local electronic environment in solution and the solid state.<sup>[37]</sup>

While pure BC has attractive optical properties, it is difficult to process because it is very brittle and weak, breaking into a powder with even gentle handling. We hypothesized that dispersing BC in a polymer matrix could maintain a high index of refraction while improving its processibility. We selected polystyrene as a candidate polymer matrix. PS is a common thermoplastic polymer with a refractive index of about 1.6 across the visible spectrum,<sup>[38]</sup> as shown in Figure 1c.

We prepared thin composite films of BC and PS by spin coating. Photographs of the samples are shown in Figure 1d. We quantified the uniformity and thickness of the films using optical profilometry, as shown in Figure 1e,f. We saw no significant difference in the roughness of the films, even at very high loadings of BC. The optical properties of a range of BC/PS films were characterized using ellipsometry. The measured refractive indices  $n(\lambda)$  and absorption lengths  $\ell_{\text{abs}}(\lambda)$  are plotted in Figure 2a. As the weight percentage of BC increases, the refractive index dispersion shows strong anomalous dispersion, that is, a pronounced dip/peak develops on either side of the absorption band. The highest, measured refractive index is 2.23 at a wavelength of 531 nm for a 67 w/w% BC/PS film.

The peak refractive index increases with the concentration of BC, as plotted in Figure 2b. At concentrations lower than 67 w/w%, the concentration dependence is roughly linear, as expected by the Equation (1) and the Clausius–Mosotti equation. The latter relates the macroscopic response of a material to the response of its molecular constituents, and anticipates departures from linear concentration-dependence at high concentrations due

to dipolar coupling between dye molecules (see e.g., ref. [39]). Nevertheless, the wavelength dependence of the refractive index of the 67 w/w% BC/PS blend is well predicted by Equation (1), as shown by the light gray curve in Figure 2c. Discrepancies could be due not only to coupling between dye molecules, but also to differences in the local electronic environment of chloroform and PS.

The Kramers–Kronig calculation for the blend’s optical properties is based on an extrapolation from the dye behavior in a dilute solution. Alternatively, we can use the law of mixtures,<sup>[40]</sup> to extrapolate the blend’s optical properties based on the measured refractive index of pure BC and PS. In this way,

$$n(\lambda) = n_{\text{BC}}(\lambda)\phi + n_{\text{PS}}(\lambda)(1 - \phi) \quad (2)$$

where  $\phi$  is the volume fraction of BC and  $n_{\text{BC}}$ ,  $n_{\text{PS}}$  are the refractive indices of pure BC and pure PS, respectively. Since BC and PS have similar density, their weight and volume fractions are essentially the same. This estimate for the refractive index is shown as a dashed curve in Figure 2c, and also matches the data reasonably well.

The possible applications of this approach for increasing the refractive index are limited by residual absorption. The intrinsic trade-off between high refractive index and absorption is captured nicely by Figure 2d, where we plot the absorption length (in units of wavelength) versus the refractive index. While the 67 w/w% BC/PS sample can reach refractive indices as high as 2.23, the absorption length at the same frequency is only about half a wavelength. This rule out any application where light propagates through the material, such as lenses. Luckily, with only a 10% decrease of the refractive index, to a value of 2.0, the absorption length increases tenfold to about five wavelengths in the material. While this may be too short for most applications, we will show below that it can be effectively exploited for nanophotonic applications.

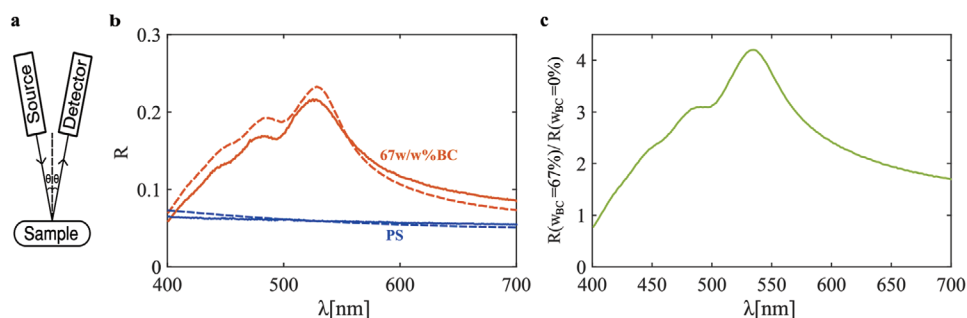


**Figure 3.** Reflectance increases significantly by incorporating BC. a) Schematic plot of the reflectance measurement set-up ( $\theta = 15^\circ$ ). b) Measured (solid lines) and modeled (dashed lines) reflectances of the 67 w/w% BC/PS film (orange) and the pure PS film (dark blue). c) Theoretical reflectances ratio of the 67 w/w% BC/PS film (57 nm) over the pure PS film (57 nm).

As an essential first step, we show that adding an absorbing material to a thin film can increase its reflectance. This may seem counterintuitive, but it is expected based on the observed increase of the index of refraction and the Fresnel equations. To demonstrate this, we compare the specular reflectance of PS and 67 w/w% BC/PS thin films in **Figure 3**. While the reflectance of the pure PS film is around 0.06 across the visible spectrum, the reflectance spectrum of the 67 w/w% BC/PS film reaches a peak value of 0.22 (**Figure 3b**), about 4× higher than the reflectance of a PS film of the same thickness (**Figure 3c**). We fitted the measured reflectance spectra to transfer-matrix calculations<sup>[41]</sup> using the measured refractive indices of both films, allowing their thickness to vary. The resulting thicknesses are 57 and 41 nm for PS and BC/PS films, respectively. The best fit spectra fit the data reasonably well. For comparison, the optical profilometer thickness measurements of the same films thickness were  $72 \pm 10$  and  $35 \pm 7$  nm for PS and BC/PS, respectively.

To demonstrate the generality of our approach, we produced thin films of ethyl cellulose EC loaded with 67 w/w% BC. EC is an attractive choice, because it is an inexpensive, commercially available, abundant plant-sourced polymer. We found very similar results to the PS films shown above, as summarized in **Figure 4**. Thin films of EC and BC/EC had similar roughness and uniformity (see **Figure 4a,b**). While pure EC has a refractive index of about 1.44 across the visible wavelength range, the refractive index of the BC/EC composite had a peak refractive index of 2.15 at 528 nm, decaying to 1.83 at 600 nm, as shown in **Figure 4c**. The specular reflection from thin films of BC/EC was almost eightfold higher than plain EC films at the peak near 529 nm (**Figure 4d,e**). It should be noted that these high refractive index films are based solely on plant-based materials.

The results above demonstrated that BC can be incorporated at high loadings in a polymer matrix to achieve a strong optical response. However, it remains to be seen whether these mixtures maintain the processability of the host polymer. We therefore tested the thermoforming ability of 40 w/w% BC/PS mixtures. For this, we made a 40 w/w% BC/PS mixture by solution casting using dichloromethane as solvent under vacuum (180 mbar) at room temperature. The resulting composite is dark orange in color (**Figure 5a**), and has a porous structure as revealed by scanning electron microscopy (SEM; **Figure 5b**). Then, we hot pressed the composite at 170 °C, which resulted in the formation of a 2 mm thick film. The resulting material

was dark green (**Figure 5c**), and no porosity was visible in SEM images (**Figure 5d**).

Differential scanning calorimetry (DSC, **Figure 5e**) and X-ray diffraction (XRD, **Figure 5f**) revealed that the BC was in a crystalline form after solution casting, but not after hot pressing. Specifically, DSC revealed a melting event in the solution-cast BC/PS sample (before hot pressing (BHP)) between 170–190 °C, matching the exothermic peak in the pure BC sample. Similarly, XRD revealed a number of sharp, crystalline

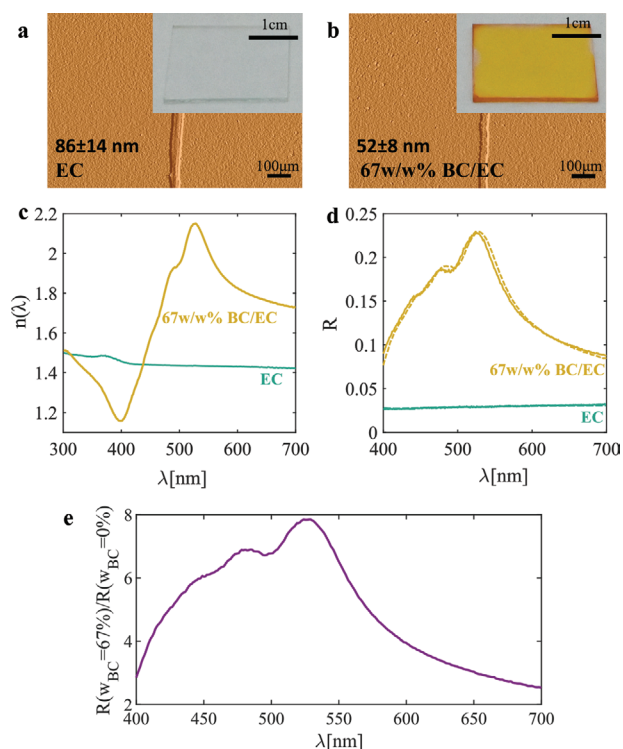


**Figure 4.** High refractive index blend of plant-based pigment, BC, and plant-based polymer, EC. a,b) Photos and surface profiles of EC and 67 w/w% BC/EC films. c) Measured refractive indices of 67 w/w% BC/EC film (orange), and pure EC (green). d) Reflectance of the 67 w/w% BC/EC film (orange) and the pure EC film (green). Measured results are in solid lines. Modeled results are in dashed lines using thicknesses of 58 and 45 nm for BC/EC and EC, respectively. e) Ratio of measured reflectance of the EC/BC film to the theoretical reflectance of a EC film with the same thickness (58 nm).

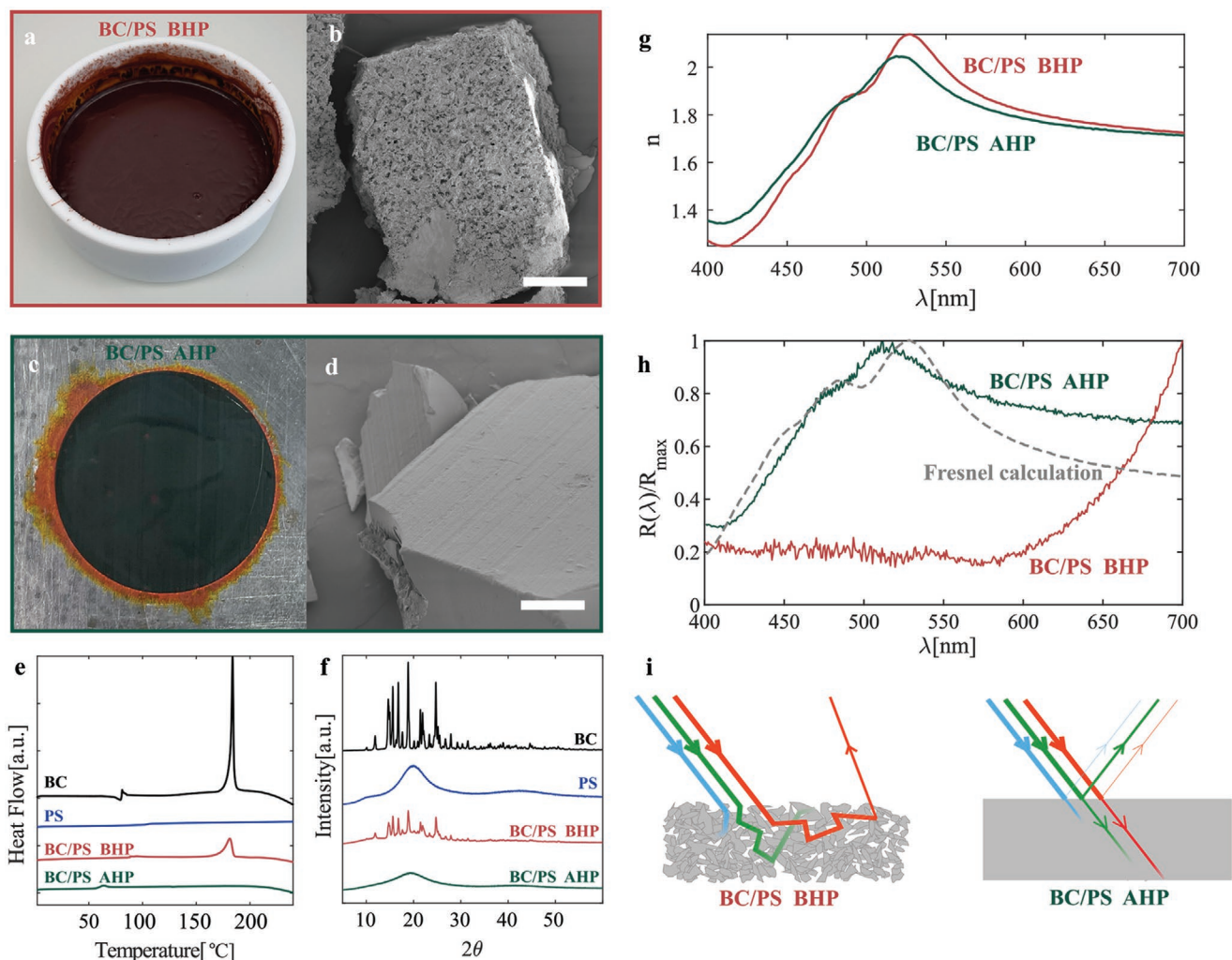


**Figure 5.** Processability, structure, and optical properties of BC/PS composites. a) Photo of 40 w/w% BC/PS mixture after solution casting, and before hot pressing (BHP). Diameter of the petri dish is 10 cm. b) SEM image of the sample. Scale bar: 200  $\mu\text{m}$ . c) Photo of 40 w/w% BC/PS composite after hot pressing (AHP) at 170  $^{\circ}\text{C}$ . Diameter of the green disc is 2.5 cm. d) SEM image of the sample after hot pressing at 170  $^{\circ}\text{C}$ . Scale bar: 200  $\mu\text{m}$ . e, f) DSC and XRD results of a 40 w/w% BC/PS mixture before (BHP) and after (AHP) hot pressing. g) Refractive index dispersions of 40 w/w% BC/PS composites before (red) and after hot pressing (green). h) Normalized reflectances of the 40 w/w% BC/PS mixture before (red) and after (green) hot pressing. Reflectance calculated by the Fresnel equations in gray, dashed line. i) Schematic of the light propagation in BC/PS films.

peaks in the solution-cast BC/PS sample that matched the diffraction peaks of pure BC. These characteristic features of crystalline BC are completely absent from the DSC and XRD results after hot pressing (AHP). We therefore conclude that hot-pressing the BC/PS film at the melting point of BC dissolves it into the PS matrix. Upon cooling, the PS vitrifies before the BC re-crystallizes, leaving a solid BC solution frozen in vitrified PS. This is particularly attractive for optical applications because molecularly dispersed pigments do not scatter light. To confirm that heat treatment did not compromise optical performance, we measure the refractive index dispersion of the hot pressed material, shown in Figure 5g, by ellipsometry on a thin film formed by spin coating after redissolving the hot-pressed sample. We observed only a slight decrease in the peak refractive index, with a maximum value of 2.04 at 520 nm. Processing at higher temperatures (230  $^{\circ}\text{C}$ ) enabled extrusion of the material into fibers, but almost entirely removed the refractive index

enhancement, as shown in the Supporting Information, likely due to a chemical decomposition of the BC.

Hot-pressing at 170  $^{\circ}\text{C}$  transforms the dark-red solution-cast mixture into a dark green material. To quantify this difference in appearance, we measured the specular reflectance of each sample, shown in Figure 5h. While the solution-cast film only reflects the longest visible wavelengths, the reflectance of the hot-pressed film closely follows the profile of its measured refractive index, which both features a peak near 520 nm. For comparison, we superimpose the Fresnel prediction for specular back-reflection as a gray curve, where  $R = |(\tilde{n} - 1) / (\tilde{n} + 2)|^2$ , where  $\tilde{n} = n + ik$  is the complex refractive index.

The appearance of the hot-pressed film is determined by its refractive index, while the color of the solution cast film is dominated by its absorption spectrum. As shown above, the solution cast film has a complex uncontrolled structure, which apparently has three phases, a PS-rich phase, BC crystals, and

air. This complex structure should strongly scatter light of all wavelengths, characterized by the transport mean-free path,  $\ell_t$ . When an absorption-free sample is much thicker than  $\ell_t$ , it appears white because each wavelength can be scattered multiple times and re-emerge from the surface. In the presence of absorption, only wavelengths with an absorption length,  $\ell_{\text{abs}}$ , much longer than  $\ell_t$  will be reflected, as shown schematically in Figure 5i. In our BC/PS samples, the absorption length increases steadily at long-wavelengths (see Figure 2a). With a presumed scattering length on the order the wavelength of light, only the longest wavelengths can be scattered enough times to be reflected from the sample. Therefore, the color of the strongly-scattering solvent-cast sample is dominated by the absorption properties of the medium. This is the same color-producing mechanism as pigmentary particles. On the other hand, hot-pressing transforms the mixture in a single phase as confirmed by SEM, DSC, and XRD measurements of Figure 5. With no internal scattering structures, the reflection is limited to the first surface, and the rest of the light propagates through the material without scattering until it is eventually absorbed, as shown schematically in Figure 5i.

So far, we have demonstrated the efficacy of enhancing the refractive index by pigment loading for simple films, where we demonstrated a strong effect on their reflectance (Figures 3, 4, and 5h). To investigate whether dye-loaded polymers could be

attractive for nanophotonic applications, we investigated the impact of dye-loading on the scattering of individual nanoparticles and the efficiency of multilayered Bragg reflectors.

To predict the influence of the refractive index enhancement on the scattering of particles made of BC/PS mixtures, we calculated the scattering and absorption properties of individual particles using Mie theory.<sup>[42]</sup> We focus on particle diameters typically used for the self-assembly of photonic crystals and glasses, 150 to 350 nm. **Figure 6a** compares the scattering efficiency,  $Q_{\text{sca}}$ , to the absorption efficiency  $Q_{\text{abs}}$ , for 67 w/w% BC/PS nanoparticles in water. The scattering (absorption) efficiency  $Q_{\text{sca}}$  ( $Q_{\text{abs}}$ ) is the ratio of the scattering (absorption) cross section to the geometrical cross section. For 350 nm diameter particles, the maximum scattering efficiency is 2.86 at a wavelength of 552 nm. While the absorption efficiency is much smaller under the same conditions, it is still significant ( $Q_{\text{abs}} = 0.56$ ). Note that  $Q_{\text{sca}}$  is a factor of five larger than the scattering efficiency of a pure PS particle at the same size and wavelength (Figure S3, Supporting Information). In *Pierid* butterflies, a similar enhancement has been observed. There, incorporation of pterin pigments increases the scattering efficiency of microparticles tenfold.<sup>[34]</sup> Further work is needed to reveal how this competition of scattering and absorption translates to the optical properties of periodic and quasi-periodic distributions of such particles in photonic crystals<sup>[43,44]</sup> and photonic glasses.<sup>[45,46]</sup>

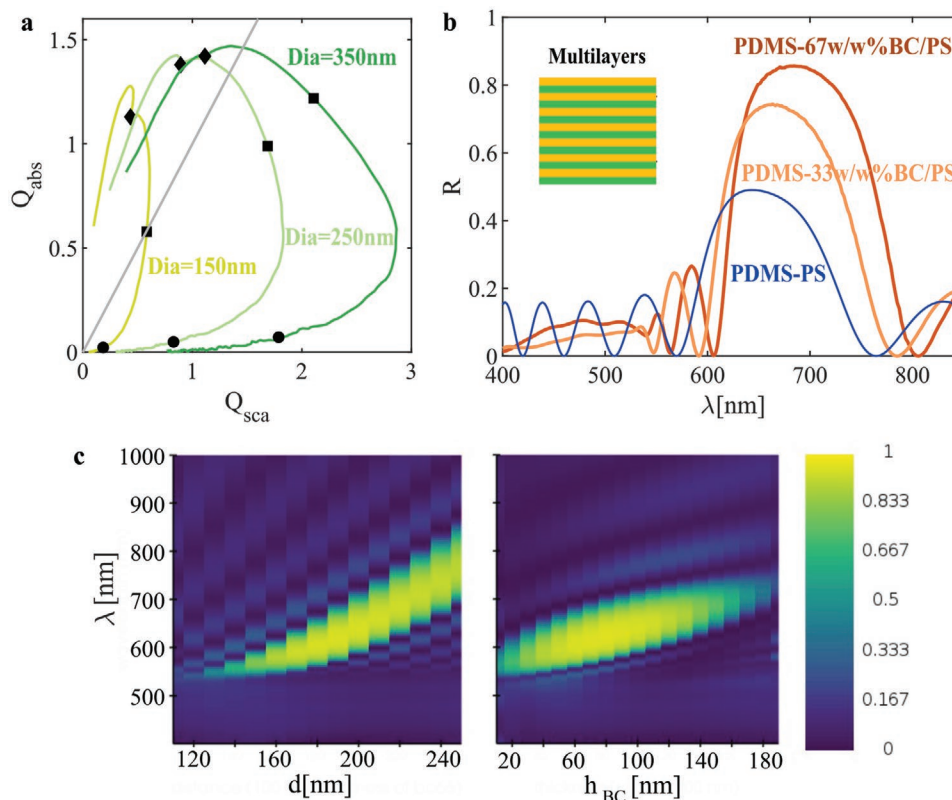


**Figure 6.** Numerical simulations of properties of nanophotonic structures made from BC/PS composites. a) Scattering efficiencies versus absorption efficiencies for 67 w/w% BC/PS particles with different diameters (Dia) in water, calculated by Mie theory. Data points for wavelengths of 500, 535, and 592 nm are marked in diamonds, squares, and circles, respectively. b) Modeled reflectances of a multilayer Bragg reflector with seven repeated layers of BC-loaded PS (thickness of each layer 100 nm) and a material with  $n = 1.4$  (thickness of each layer 120 nm). c) Reflectances of seven-repeat multilayers of 67 w/w% BC/PS and a material with  $n = 1.4$ , where the thicknesses of the layers are varied. In the left panel, the thickness of the BC/PS layer,  $h_{\text{BC}}$  is fixed at 100 nm and total thickness of each repeat unit,  $d$ , is varied. In the right panel,  $d$  is fixed at 200 nm and  $h_{\text{BC}}$  is varied.

Putting aside the complexity of single particle response, we can assess the impact of absorption-enhanced scattering in a 1D periodic structure, the multilayer Bragg reflector (MBR),<sup>[47]</sup> shown schematically in Figure 6b. We investigated the optical response of a multilayer with seven alternating layers of two materials. One layer has a refractive index of 1.4 (e.g., PDMS), and the second has the refractive index dispersion of our BC/PS mixture (see e.g., refs. [48,49]). Keeping the layer thicknesses fixed (120 nm for the low index material, and 100 nm for BC/PS blends), we varied the loading of BC from 0% to 67% and calculated the reflectance spectrum of the structure at normal incidence, shown in Figure 6b. Without further optimization, the peak reflectance increases from 0.48 with pure PS up to 0.85 with 67 w/w% BC/PS. Varying the thickness of the layers, the reflectances of this system can reach as high as 0.95, as shown in Figure 6c. We observe a cut-off effect for smaller lattice spacings. As the reflectance peak reaches the absorption band, it first narrows and then fully disappears. Specifically, the reflectance peak width is around 100 nm for  $d = 180$  nm, narrowing to 50 nm for  $d = 160$  nm.

### 3. Conclusion

We have shown that BC can be dispersed in PS and EC at very high loadings. These mixtures can reach refractive indices over two for a range of wavelengths, and display enhanced reflectance in films. Composites of BC and PS maintain their thermoforming ability. Thermoforming has an additional benefit: it dissolves BC crystals, removing uncontrolled scattering from crystallized pigment. Numerical calculations suggest that the enhancement of refractive index due to the addition of dye can significantly enhance scattering by nanoparticles and improve the reflectance of Bragg reflectors.

This work demonstrates a new degree of freedom for the design of photonic nanostructures, enabling the enhancement of refractive index at specific wavelengths. Our theoretical results on Bragg reflectors suggest this strategy is particularly effective when wavelengths with strongly-enhanced refractive indices overlap with the wavelengths selected by the nanostructure. This work demands further development of the theory of light transport in nanostructures with simultaneous scattering and absorption.

To realize the photonic nanostructures proposed here, several challenges in materials chemistry and processing must be overcome. For example, new synthetic approaches are required to produce monodisperse polymer nanoparticles with high dye loadings. Finally, our proof-of-concept pigment,  $\beta$ -carotene, is prone to oxidation, and strategies to stabilize it would greatly improve the longevity of these materials. This could include the use of polymer matrices with low oxygen permeability.

### 4. Experimental Section

**Materials:** BC (synthetic,  $\geq 93\%$  (UV)), PS (35 kDa (used for making films atop silicon wafers and glass slides) and 192 kDa (used for processability experiments)), EC (48.0–49.5% w/w ethoxyl basis),

chloroform and dichloromethane were bought from Sigma-Aldrich and used as received.

**UV-Vis Spectrometry:** The absorption spectrum of chloroform and BC solution in chloroform (0.1 mM) was recorded by a UV-vis spectrophotometer (Agilent Cary 60). The absorbance of chloroform was subtracted from the absorbance of BC solution in order to have absorbance of pure BC. This absorbance data was used to calculate the molar extinction coefficient of BC according to the Beer-Lambert law.

**Film Preparation:** To a weighed amount of PS or EC, the BC was added according to w/w% (Table S1, Supporting Information). A solution of this mixture in chloroform at a given concentration (Table S1, Supporting Information) was stirred at 800 rpm under dark at room temperature. This solution was filtered through a 0.45  $\mu\text{m}$  filter and the film was spin coated at 1000 rpm for 10 min over silicon wafer (size:  $2 \times 2 \text{ cm}^2$ ) or glass slide (size:  $2.5 \times 2.2 \text{ cm}^2$ ). The volume of solution taken for spin coating was 250 or 300  $\mu\text{L}$  for silicon wafer or glass slide, respectively. Specific compositions of solutions used for spin coating are found in the Supporting Information. The measurements of refractive index and reflectance on these spin-coated films were done within few hours (1–2 h) after preparation. The films were stable when stored in an oxygen-free environment, but degraded within 24 h when stored in air.

**Profilometry:** The imaging of the films using a 3D optical profilometer (S neox) using 10 $\times$  DI lens. In order to know the thickness of the films, a cut was made in the film using blade to scrap the portion of the material. The difference between the heights of the planes with and without the material gave the thickness of the films.

**Ellipsometry:** For refractive index measurements, a spectroscopic ellipsometer (M2000, J. A. Woollam) was used to measure the phase and amplitude change of light after interacting with the samples. All measurements were performed between 250 and 1000 nm at an angle of incidence 65 $^\circ$ , and all data were acquired and analyzed using WVASE software. Since the films were transparent at longer wavelengths, the films were regarded as a homogeneous material with the thickness fitted by Cauchy dispersion relation in the wavelength range from 600 to 1000 nm. After the film thickness was determined and fixed, the optical constants, refractive indices  $n$  and extinction coefficient  $\kappa$  were fitted using point to point fitting mode.

**Reflectance Measurement:** The specular reflectance of the films had been measured with an angle-resolved spectrophotometry setup. The light source was a deuterium-halogen lamp (Ocean Optics DH-2000-BAL), ranging from 200 to 1000 nm. The sample was placed on a rotating stage and could be tilted to the desired angles. Finally, a light detector (Ocean Optics, QE Pro) was mounted on a rotating arm, which was controlled by software. The incident angle was set to be 15 $^\circ$  and the specular reflectance was measured. The reflectance was calculated using reflection from a broadband dielectric mirror (Thorlabs, BBSQ2-E02) at the same incident angle as reference. During the reflectance measurement, a layer of translucent Scotch tape was applied on the back side of the glass substrate to suppress unwanted back reflection from the glass-air interface.

**Optical Modeling:** The measured reflectances of thin films were fitted by a transfer matrix method based on the RTAcalc code developed by A. Rose. It was assumed the films are in air and on a semi-infinite glass substrate in the modeling.

The Mie scattering calculations were done using the open source MATLAB code developed by Christian Mätzler.

The reflectances of multilayer were simulated with 3D finite-difference time-domain (FDTD) calculations using Lumerical FDTD Solutions, a commercial-grade Maxwell equation solver.

**XRD Measurement:** Samples were finely ground into powders before the XRD measurements. The XRD measurements were performed on the Panalytical X'Pert PRO MPD diffractometer with Cu K $\alpha$  (8.04 keV) radiation.

**DSC Measurement:** The DSC measurements of the samples were performed on TA DSC2500 with a ramping speed of 10 $^\circ\text{C min}^{-1}$  under inert atmosphere.

**Scanning Electron Microscopy:** The SEM observations were performed on the Hitachi SU5000.



## Supporting Information

Supporting Information is available from the Wiley Online Library or from the author.

## Acknowledgements

M.Y. and T.S. contributed equally to this work. The authors thank Kiril Feldman for assistance with polymer processing and DSC measurements, Thomas Weber for help with XRD, Hui Cao for feedback on the optical data and Carla Fernandez-Rico for comments on the manuscript. This work was financially supported by the Swiss National Science Foundation through the NCCR Bio-inspired Materials.

## Conflict of Interest

The authors declare no conflict of interest.

## Data Availability Statement

The data that support the findings of this study are available from the corresponding author upon reasonable request.

## Keywords

high refractive index, plant-based products, polymers, structural color

Received: May 26, 2021

Revised: July 14, 2021

Published online: September 23, 2021

- [1] C. Paquet, E. Kumacheva, *Mater. Today* **2008**, *11*, 48.  
 [2] J.-g. Liu, M. Ueda, *J. Mater. Chem.* **2009**, *19*, 8907.  
 [3] T. Badur, C. Dams, N. Hampp, *Macromolecules* **2018**, *51*, 4220.  
 [4] H. Jiang, X. Pan, N. Li, Z. Zhang, J. Zhu, X. Zhu, *React. Funct. Polym.* **2017**, *111*, 1.  
 [5] T. S. Kleine, N. A. Nguyen, L. E. Anderson, S. Namnabat, E. A. LaVilla, S. A. Showghi, P. T. Dirlam, C. B. Arrington, M. S. Manchester, J. Schwiegerling, R. S. Glass, K. Char, R. A. Norwood, M. E. Mackay, J. Pyun, *ACS Macro Lett.* **2016**, *5*, 1152.  
 [6] J. L. H. Chau, Y.-M. Lin, A.-K. Li, W.-F. Su, K.-S. Chang, S. L.-C. Hsu, T.-L. Li, *Mater. Lett.* **2007**, *61*, 2908.  
 [7] C. Lü, B. Yang, *J. Mater. Chem.* **2009**, *19*, 2884.  
 [8] P. Tao, Y. Li, A. Rungta, A. Viswanath, J. Gao, B. C. Benicewicz, R. W. Siegel, L. S. Schadler, *J. Mater. Chem.* **2011**, *21*, 18623.  
 [9] A. K. Yetisen, Y. Montelongo, H. Butt, *Appl. Phys. Lett.* **2016**, *109*, 061106.  
 [10] K.-C. Kim, *Mater. Lett.* **2015**, *160*, 158.  
 [11] D. P. Sanders, *Chem. Rev.* **2010**, *110*, 321.  
 [12] T. Higashihara, M. Ueda, *Macromolecules* **2015**, *48*, 1915.  
 [13] D.-P. Song, C. Li, W. Li, J. J. Watkins, *ACS Nano* **2016**, *10*, 1216.  
 [14] M. A. Olshavsky, H. R. Allcock, *Macromolecules* **1995**, *28*, 6188.  
 [15] D. H. Kim, W. Jang, K. Choi, J. S. Choi, J. Pyun, J. Lim, K. Char, S. G. Im, *Sci. Adv.* **2020**, *6*, eabb5320.  
 [16] L. Fang, J. Sun, X. Chen, Y. Tao, J. Zhou, C. Wang, Q. Fang, *Macromolecules* **2020**, *53*, 125.  
 [17] M. R. Bockstaller, E. L. Thomas, *J. Phys. Chem. B* **2003**, *107*, 10017.  
 [18] L. Zimmennann, M. Weibel, W. Caseri, U. W. Suter, *J. Mater. Res.* **1993**, *8*, 1742.  
 [19] R. J. Gehr, R. W. Boyd, *Chem. Mater.* **1996**, *8*, 1807.  
 [20] T. Hanemann, K. Honnef, *J. Appl. Polym. Sci.* **2011**, *122*, 3514.  
 [21] T. Hanemann, K. Honnef, *J. Appl. Polym. Sci.* **2014**, *131*, 9.  
 [22] J. Böhm, J. Haußelt, P. Henzi, K. Litfin, T. Hanemann, *Adv. Eng. Mater.* **2004**, *6*, 52.  
 [23] T. Magrini, F. Bouville, A. Lauria, H. L. Ferrand, T. P. Niebel, A. R. Studart, *Nat. Commun.* **2019**, *10*, 2794.  
 [24] V. Lucarini, *Kramers–Kronig Relations in Optical Materials Research*, Springer, Berlin **2005**.  
 [25] G. T. Reed, G. Mashanovich, F. Y. Gardes, D. J. Thomson, *Nat. Photonics* **2010**, *4*, 518.  
 [26] M. A. Foster, A. C. Turner, J. E. Sharping, B. S. Schmidt, M. Lipson, A. L. Gaeta, *Nature* **2006**, *441*, 960.  
 [27] C. Schinke, P. Christian Peest, J. Schmidt, R. Brendel, K. Bothe, M. R. Vogt, I. Kröger, S. Winter, A. Schirmacher, S. Lim, H. T. Nguyen, D. MacDonald, *AIP Adv.* **2015**, *5*, 067168.  
 [28] J.-H. Huh, J. Lee, S. Lee, *Nano Lett.* **2020**, *20*, 4768.  
 [29] G. E. Hill, K. J. McGraw, *Bird Coloration: Mechanisms and Measurements*, Vol. 1, Harvard University Press, Cambridge, MA **2006**.  
 [30] S. Yoshioka, S. Kinoshita, *Phys. Rev. E* **2011**, *83*, 051917.  
 [31] D. G. Stavenga, H. L. Leertouwer, D. C. Osorio, B. D. Wilts, *Light: Sci. Appl.* **2015**, *4*, e243.  
 [32] A. Kawamura, M. Kohri, G. Morimoto, Y. Nannichi, T. Taniguchi, K. Kishikawa, *Sci. Rep.* **2016**, *6*, 33984.  
 [33] M. Xiao, Z. Hu, Z. Wang, Y. Li, A. D. Tormo, N. Le Thomas, B. Wang, N. C. Gianneschi, M. D. Shawkey, A. Dhinojwala, *Sci. Adv.* **2017**, *3*, e1701151.  
 [34] B. D. Wilts, B. Wijnen, H. L. Leertouwer, U. Steiner, D. G. Stavenga, *Adv. Opt. Mater.* **2017**, *5*, 1600879.  
 [35] B. A. Palmer, V. J. Yallapragada, N. Schiffmann, E. M. Wormser, N. Elad, E. D. Afalo, A. Sagi, S. Weiner, L. Addadi, D. Oron, *Nat. Nanotechnol.* **2020**, *15*, 138.  
 [36] T. Sai, M. Saba, E. R. Dufresne, U. Steiner, B. D. Wilts, *Faraday Discuss.* **2020**, *223*, 136.  
 [37] N. Gong, Z. Li, C. Sun, Z. Men, *Progress in Carotenoid Research* **2018**.  
 [38] N. Sultanova, S. Kasarova, I. Nikolov, *Acta Phys. Pol., A* **2009**, *116*, 585.  
 [39] K. Kim, S. Yoo, J.-H. Huh, Q.-H. Park, S. Lee, *ACS Photonics* **2017**, *4*, 2298.  
 [40] W. Heller, *J. Phys. Chem.* **1965**, *69*, 1123.  
 [41] K. J. Pascoe, Reflectivity and Transmissivity through Layered, Lossy Media: A User-Friendly Approach, Technical Report, Air Force Institute of Technology, School of Engineering, Wright-Patterson Air Force Base, OH **2001**.  
 [42] C. F. Bohren, D. R. Huffman, *Absorption and Scattering of Light by Small Particles*, John Wiley & Sons, Hoboken, NJ **2008**.  
 [43] C. López, *Adv. Mater.* **2003**, *15*, 1679.  
 [44] J. D. Joannopoulos, P. R. Villeneuve, S. Fan, *Nature* **1997**, *386*, 143.  
 [45] S. Magkiriadou, J.-G. Park, Y.-S. Kim, V. N. Manoharan, *Phys. Rev. E* **2014**, *90*, 062302.  
 [46] L. Schertel, L. Siedentop, J.-M. Meijer, P. Keim, C. M. Aegerter, G. J. Aubry, G. Maret, *Adv. Opt. Mater.* **2019**, *7*, 1900442.  
 [47] Y. Fink, J. N. Winn, S. Fan, C. Chen, J. Michel, J. D. Joannopoulos, E. L. Thomas, *Science* **1998**, *282*, 1679.  
 [48] M. Kolle, A. Lethbridge, M. Kreysing, J. J. Baumberg, J. Aizenberg, P. Vukusic, *Adv. Mater.* **2013**, *25*, 2239.  
 [49] M. Kolle, B. Zheng, N. Gibbons, J. J. Baumberg, U. Steiner, *Opt. Express* **2010**, *18*, 4356.